

Low cost agroindustrial biomasses and ferromagnetic bionanocomposites to cleanup textile effluents

Geórgia Labuto^{1*}, Débora Selene Cardona¹, Karina Bugan Debs¹, Augusto Ribeiro Imamura¹, Katia Crystina Hipólito Bezerra², Elma Neide Vasconcelos Martins Carrilho³, Paula Silvia Haddad¹

¹Departamento de Química, Universidade Federal de São Paulo, Diadema, CEP 09913-030, São Paulo, Brazil.

²Faculdade de Tecnologia SENAI Antônio Skaf, Rua Correia de Andrade Street, CEP 03008-020, São Paulo, Brazil.

³Departamento de Ciências da Natureza, Matemática e Educação, Universidade Federal de São Carlos, CEP 13600-970 Araras – São Paulo, Brazil.

Keywords: yeast biomass, cork, reactive dyes, modeling, standard errors (SE), choose an isotherm model

Corresponding author email: geolabuto@gmail.com, tel: +55 11 976366085

Abstract

The introduction of textile dyes in the environment is a great concern since they can be composed by organic and inorganic recalcitrant and/or toxic compounds. In the present work we synthesized, characterized and applied ferromagnetic nanocomposites prepared from two agroindustry residues, cork powder (CP) and yeast biomass (YB), for dye adsorption. The CP, YB, ferromagnetic nanoparticles (MNP) and the ferromagnetic nanocomposites powdered cork (CP-MNP) and yeast biomass from ethanol industry (YB-MNP) were evaluated as sorbents for methylene blue, a cationic dye with known chemical structure. All sorbents were applied to cleanup dyed cotton fabric effluents, containing the reactive dye trichomy (Yellow CL-2R, Red CL-5B and Blue HF-RL, all Drimaren). The experimental sorption capacities (SC_{exp}) of these sorbents for methylene blue were 36.39 ± 0.38 mg/g (CP), 33.61 ± 0.94 mg/g (CP-MNP), 27.73 ± 0.27 mg/g (YB), 30.42 ± 0.85 mg/g (YB-MNP), and 2.91 ± 0.41 mg/g (MNP). A proposed decision algorithm was employed to choose the isotherms model best fit to each process for which we found CP-MNP (Langmuir), CP (Langmuir), YB-MNP (SIPS), YB (SIPS), and MNP (Freundlich). High sorption efficiency was found, reaching up recoveries of $50.0 \pm 0.8\%$ (CP), $66.48 \pm 0.01\%$ (CP-MNP), $85.93 \pm 0.07\%$ (YB), and $82.6 \pm 0.1\%$ (YB-MNP) of dyes residues. This suggests that these materials have great potential to treat dyes effluents from textile industries.

1. Introduction

The textile industry is one of the largest polluters of water. In 2002, around 10,000 different dyes and pigments were used by this production sector, with a world consumption of 7×10^5 tons, being project a growth of 3.6% per year [1]. The treatment of dyes effluent frequently employs sludge tanks enabled for remediation, which requires the control of microorganisms, dispenses considerable time in treatment, can generate bioproducts even more toxic than the treated effluent and need landfills for sludge disposal [2]. Physical, chemical and electrochemical, including oxidative degradation, coagulation, membrane filtering, ozonation and sorption have been reported [2, 3, 4]. In case of sorption methods, the use of biomasses increases bio-economy since many biosorbents employed are residues from a variety of processes, and present high sorption capacities for both inorganic and organic species [5-7].

Moreover, nanoparticles have been associated with biosorbents to increase their sorption capacities and enrich them with new characteristics such as superparamagnetic properties from the formation of composites with ferromagnetic nanoparticles [8]. Great advantages of composites are their superparamagnetic characteristic from the nanoparticles, which allow an easy removal of the adsorbent from water using a magnet, and the organic functional groups on the biomasses, which improve their sorption capacities for contaminants uptake [9]. Besides, these hybrid materials can enhance the biomasses that are often agroindustrial wastes, or that have low market value [10].

In the recent years, composites of magnetic materials prepared from different biomasses were reported to remove dyes from single solutions [8, 11-15]. In these researches, methylene blue was studied, since it is a reference and has a known chemical structure. Despite the high sorption capacities reported the shortcomings of the majority of the articles in this area, according to Tim [16], is the absence of reports about the treatment of real effluents, which are composed by a mixture of dyes (frequently a trichomy). Besides, factories effluents commonly present hydrolyzed dyes and other components employed in the dyeing processes.

In this way, we synthesized and characterized three sorbent materials: ferromagnetic nanoparticles (MNP), yeast biomass (from ethanol industry) ferromagnetic bionanocomposite (YB-MNP) and cork powder ferromagnetic bionanocomposites (CP-MNP). The use of magnetic materials, yeast biomass (YB), and cork powder (CP) was evaluated for the sorption of methylene blue and a cationic dye effluents from a textile pilot plant factory. In addition, we propose a decision algorithm to choose the best-fit adsorption isotherm model.

2. Methods

2.1. Synthesis of nanoparticles and bionanocomposites

Yeast biomass residues (YB) were donated from an alcohol-producing industry of the state of São Paulo, in Brazil, and the cork powder (CP) was bought from a company that produces cork artifacts, and defines it as a waste in their processes. The synthesis of MNP was carried out using a co-precipitation method [17], which consisted of a mixture of $\text{FeCl}_3 \cdot 6\text{H}_2\text{O}$ (4.0 mL) and $\text{FeCl}_2 \cdot 4\text{H}_2\text{O}$ (1.0 mL) both prepared in 1.0 mol/L HCl. This mixture was stirred for 30 min while 200 mL of NH_4OH (0.7 mol/L) were slowly added through a burette. The resulting suspension containing magnetite nanoparticles (MNP) was centrifuged, and the magnetic precipitate was decanted and washed with purified water, followed by a rinsing with absolute ethanol and dried in a desiccator. A procedure adapted from Panneerselvam [18] was employed to produce the ferromagnetic nanocomposites of yeast biomass from ethanol industry (YB-MNP) and cork powder (CP-MNP). Thus, the procedure described to produce MNP was carried out except that the suspension was heated up to 80°C before adding 2 g of the biomass for each 250 mg of MNP. This suspension was stirred by 30 min at 80°C, and the nanocomposites were washed with absolute ethanol and reserved in desiccator for posterior use.

2.2. Characterization of nanoparticles, precursors and bionanocomposites

Elemental analysis the Flash EA 1112 Series equipment (Thermo Scientific, USA) was used to determine CHN amounts in all studied materials. Scanning Electron Microscopy images (SEM) were performed on a EVO MA 15 (Zeiss, Germany) and all measurements were made at the variable pressure (low vacuum). The secondary electron detector suitable for measurements with variable pressure was used. The voltage was 10 kV and 20 kV, and the current ranged from 21 pA to 240 pA, according to the material to be analyzed. An X-Ray (STADI-P, Stoe, Germany) was employed to obtain the diffractograms for all materials on the following parameters: The X-ray source was Mo K α 1 ($\lambda = 0.7093 \text{ \AA}$) Of 40 kV and 40 mA current, with primary beam monochromator (Ge (111) curved crystal). The detector used in the data collection was the Mythen 1K (Dectris, Switzerland) silicon strip, scanning (angle 2Θ): 12° to 100°, with angle increment: 0.015°. The FT-IR spectra were acquired in a IR Prestige-21 (Shimadzu, Japan) by KBr pellet method. The KBr pellet was used as reference (blank) to clear the apparatus and 32 scans with 4 cm⁻¹ spectral resolution were performed for all samples. The magnetization curves were obtained in Quantum Design MPMS 5XL SQUID Magnetometer device (MPMS XL7, USA). Measurements were performed on dry powder, which was lightly pressed and packed into cylindrical Lucita supports. The calibration of the equation was performed using nickel oxide ($\mu_s = 1,332 \text{ emu/g}$). The zeta potential was determined using the Zetasizer Nano Series equipment (Malvern, UK).

2.3. Dye Effluent generation process

Textile effluent (TE) was prepared by dyeing 5 g of 100% cotton fabric (180 g/m²) previously bleached, which was performed with a solution bath containing 3 primary colors composed by bifunctional cationic dyes (0.4% Drimaren Yellow CL-2R, 0.4% Drimaren Red CL-5B and 0.4% Drimaren Blue HF-RL, all Clariant S/A) and 1 mg/L sequestrant for Ca²⁺ and Mg²⁺ (Ladiquest), 65.0 g/L NaCl + 5 g/L Na₂CO₃ + 1.5 mL/L NaOH 50°βe. The dyeing procedure was executed according to the dyes manufacturer's recommendation employing a proportion of 1:10 of fabric mass and total bath volume in a dyeing machine that works at high temperature (model ALT-B, Mathis). The dyeing process was started at room temperature with the addition of 42.75 mL of potable water containing the dyes and NaCl. The temperature was raised to 60 °C (1 °C/min). After 20 min, the addition of the alkalis Na₂CO₃ and NaOH was performed in three steps of 10 min intervals, up to 30 min total. Thereafter, the temperature was maintained (40 min) to promote the fixation of the dyes in the fabric. In this industrial process, at the end of dyeing, the fabric was washed at 1:20 baths (5 g of fabric to 100 ml of wash solution) in the same dyeing equipment, 4 times. The first wash was carried out for 5 min at room temperature with acetic acid (2 ml for each litter of effluent) to neutralize the alkalis added in the dyeing step. The effluent from the first wash was collected and the fabric was twice washed (15 min at boiling) with 1 g/L of a dispersant detergent solution (Clariant S/A) to remove all hydrolyzed dyes. The effluents from these washings were also collected. The last wash was performed with potable water (5 min at room temperature) to remove chemical residues. The effluent from it was added to the previous ones, and the resulting mixture (textile effluent, TE) was homogenized and stored in an amber glass bottle under refrigeration before use. The amount of dyes remaining in the TE was analyzed by UV-Vis spectrometry UV-1280 (Shimadzu, Japan) at 586 nm employing an analytical curve built from appropriated dilution of a simulated dyeing solution containing all reagents of the effluent at the same proportions.

2.4. Evaluation of methylene blue adsorption

A 5-mL aliquot of a work solution containing 50 mg/L of methylene blue 82% purity (Sigma-Aldrich, Germany) was added to 30 mg of each sorbent material (CP; CP-MNP; YB; YB-MNP or MNP). First, these suspensions were

shacked at 200 rpm for 15 min at 25°C, after which the ones containing only CP or YB were centrifuged (6 min at 4000 rpm) and the supernatants were analyzed by UV-1280 spectrometer (Shimadzu, Japan) at 666 nm to determine the residual dye after sorption. The suspensions containing the magnetic materials (CP-MNP, YB-MNP, and MNP) were submitted to a didymium magnet to maintain the sorbent materials into the flask while the supernatants were transferred to another flask to determine the remaining dye at the same conditions. Then a new aliquot of 5 mL of the working solution was added onto the same sorbent mass, and the stirring and separation of the supernatant was again conducted. This procedure was repeated until the concentration of methylene blue determined in the supernatant after contact with the sorbent materials was the same as the working solution, denoting the saturation of the material.

The SC_{exp} averages were compared by employing one-way ANOVA and Tukey's test was applied ($\alpha = 0.05$). Thus, isotherms were constructed by plotting the experimental values of C_e (concentration of methylene blue in supernatant at equilibrium, mg/L) \times Q_e (methylene blue removed by the adsorbent, mg/g) and non-linear isotherm models were fitted on experimental data to compare the sorption performance. The non-linear methods minimize the error distribution between the experimental and theoretical isotherm [4, 19]. All the model parameters were evaluated by non-linear regression using Origin 8.0 software. All experiments were conducted in triplicate.

2.5. Textile effluent treatment

First, an analytical curve was made from the trichrome solution (400 mg/L) before the coloring process. Then, the textile effluent was analyzed by UV-Vis and the total dyes concentration of trichromy was 50 mg/L. Knowing the mass of the dyes present in the effluent, the initial mass of the sorbent was established to evaluate its treatment, based on the SC_{exp} obtained in the studies with methylene blue and that theoretically would be able to remove the same mass of the effluent. Thus, 25 mg of each sorbent material (CP; CP-MNP; YB; YB-MNP or MNP) was added to 20 mL of textile effluent and the suspensions were shacked by 15 min at 200 rpm and 25°C. After that, the suspensions with no magnetic materials (CP and YB) were centrifuged (6 min at 4000 rpm) and the supernatants were separated and analyzed employing a spectrometer UV-1280 (Shimadzu, Japan) at 584 nm to determine the residual dyes after treatment. The suspensions containing the magnetic materials (CP-MNP and YB-MNP) were submitted to a didymium magnet to maintain the sorbent materials into the flask while the supernatants were transferred to another flask to determine the remaining dyes by UV-Vis at the same conditions. Stating a partial removal of dyes from effluent, the process was repeated employing a new aliquot of effluent and higher mass of each sorbent. The employed masses were 25, 50, 150 and 300 mg. Due to the poor SC_{exp} obtained for MNP in the methylene blue sorption studies, this material was not employed in textile effluent treatment.

3. Results and discussions

3.1. Characterization of nanoparticles and bionanocomposites

Figure 1 depicts the morphology of MNP, CP, and YB, as well as the nanoparticles deposited in the reentrances of the surfaces of CP-MNP and YB-MNP. It is possible to observe that YB-MNP shows larger MNP coverage than CP-MNP. This may have occurred due to the considerably smaller size of the inactivated yeast cells than the structures of CP.

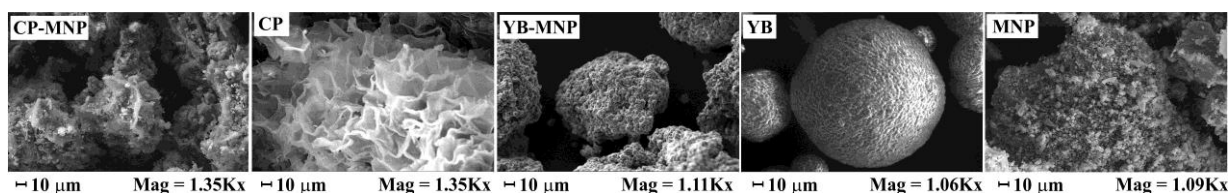


Figure 1. SEM images of CP (cork powder), CP-MNP (ferromagnetic nanocomposites of cork powder), YB (yeast biomass), YB-MNP (ferromagnetic nanocomposites of yeast biomass and MNP (magnetite nanoparticles)).

Figure 2A show the XRD profiles of YB-MNP and CP-MNP, respectively. These diffractograms exhibit six reflex peaks that are in agreement with the known reflex positions of magnetite ($2\theta = 13.7^\circ, 16.1^\circ, 19.4^\circ, 23.8^\circ, 23.3^\circ, 27.6^\circ$) due to the 220, 311, 400, 422, 511, and 440 lattice planes, respectively, of the face centered cubic lattice structure (JCPDS – PDF, 19-0629) [6] confirming that the structure is Fe_3O_4 . The inverse spinel structure consists of oxide ions in the cubic close packed organization in which 1/3 of tetrahedral interstices and 2/3 of octahedral interstices coordinate with oxygen where Fe^{2+} ions occupy the octahedral interstices, and half of the Fe^{3+} occupies the tetrahedral interstices with the remaining half of Fe^{3+} in octahedral interstices. An average crystallite size of 15 nm was calculated from the Scherrer equation [20] based on the (311) Bragg reflection. These diffractograms demonstrate that capping nanoparticles

with YB and CP did not lead to any phase change of the MNP.

An important feature of magnetite (Fe_3O_4) nanoparticles for these applications, is the superparamagnetic behavior, acting as a single magnetic domain, at temperatures above the blocking temperature [21]. The magnetization curves (Figure 2B) reveals that the residual magnetization and coercive forces were found to be zero, which confirmed the superparamagnetic characteristics of each magnetic synthesized material (neither hysteresis nor magnetic remanence was observed). The saturation magnetization (M_s) values observed for composites at room temperature were 40 and 12 emu/g for PC-MNP and YB-MNP, respectively. Which showed that the addition of the NP layer on the surface of biomasses produces a saturation magnetization comparable with that found for MNP (58 emu/g) [22]. Despite de minor value presented by composites than MNP, this behavior reveals that these both systems can be transported by an external magnetic field.

The zeta potential for CP-MNP, CP, YB-MNP, YB and MNP, and YB-MNP were -12.2 ± 0.3 , -8.6 ± 0.2 , -13.9 ± 0.5 , -9.39 ± 0.86 , $+20.3 \pm 0.4$ mV, respectively, indicating a good colloidal stability of these materials in water, with low chances to agglomerate. The zeta potential also indicates that the surface of biomasses and composites were negatively charged while MNP was positively charged, indicating that they can adsorb positively charged species.

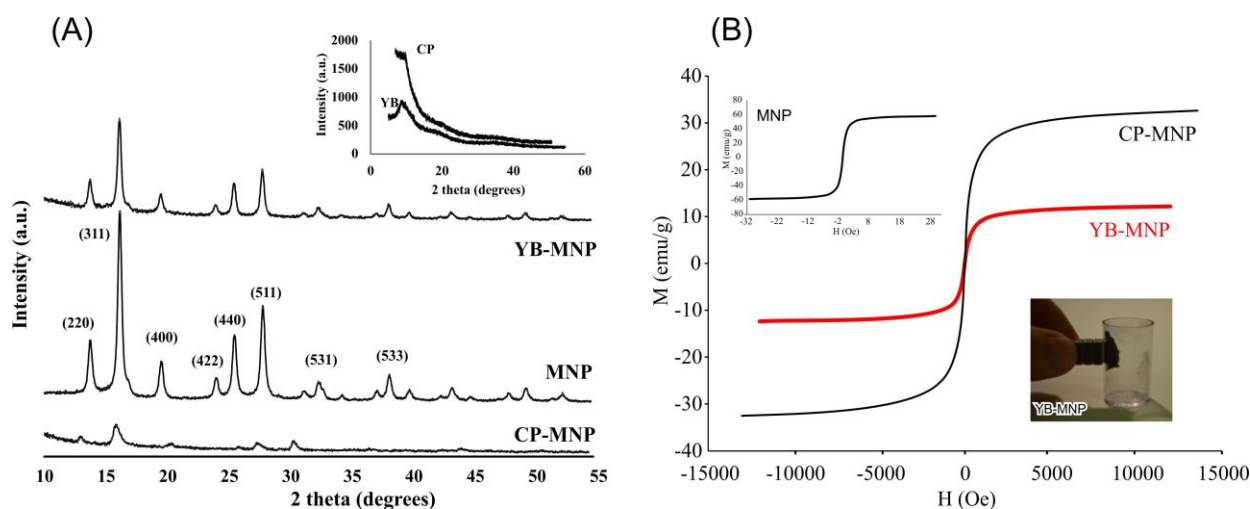


Figure 2. A) Powder X-ray diffractograms from CP (cork powder), CP-MNP (ferromagnetic nanocomposites of cork powder), YB (yeast biomass), YB-MNP (ferromagnetic nanocomposites of yeast biomass) and MNP (magnetite nanoparticles), displaying the Bragg peak reflections of magnetite for the magnetic adsorbents. B) Susceptibility of magnetization curves for CP-MNP, YB-MNP and MNP and an illustrative picture of YB-MNP being attract by a magnet.

The results of elemental were: CP) 63.5% C, 8.21% H and 1.00% N; CP-MNP) 41.81% C, 5.55% H and 1.03% N; YB) 41.0% C, 6.21% H and 6.14% N; YB-MNP) 29.7% C, 4.3% H and 3.8% N and; MNP) 3.5% C, 0.40% H and 1.00% N. These amounts denoted that he composites present a minor contribution of carbon than the precursor biosorbents, probably due to the contribution of MNP in the weighted masses used for the elemental analysis. It is also possible to observe a small carbon presence in MNP attributed to the remnants of ethanol used in the washing step of the nanoparticles after the synthesis.

The FT-IR spectra for all studied materials are shown in Figure 3. As expected, MNP shows the Fe-O stretching peak at 580 cm^{-1} and 3230 cm^{-1} , clearly identified, and not present peaks or bands that could be attributed to organic functional groups capable like the biomasses precursor of composites. For PC were observed bands at 3429 cm^{-1} (OH-bond) and at 2920 cm^{-1} (aliphatic group CH), and the stretches at 1732 cm^{-1} (C = O esters bonds) and 1620 cm^{-1} (C= bonds), These groups are present in the suberin and lignin structures that make up, respectively, 45 and 27% of cork [24] and they are amenable to the sorption of positively charged species such as reactive dyes [23]. Comparing the spectra of the precursors with the PC-MNP composite, we observed the presence of groups of both PC and MNP with emphasis on the stretching at 1732 cm^{-1} , related to Fe-O bond, of which is an indication that MNP is incorporated to PC.

Similarly, YB presented this kind of groups denoted by 1040 cm^{-1} (-C-C-group); 1233 cm^{-1} (N-O stretching); 1402 cm^{-1} (-OH stretching); 1529 cm^{-1} (bending -N-H); 1630 cm^{-1} (-C=O stretching); 2850 cm^{-1} and 2924 cm^{-1} (both attributed to aliphatic -C-H) and 3230 cm^{-1} (N-H stretching and bending O-H). Also the YB-MNP presented the same chemical groups, which are responsible for removing substances from solution [25]. However, YB-MNP also shows a

peak in 580 cm^{-1} , related to Fe-O stretching, and an intensification of the band in 3230 cm^{-1} due to hydroxyl groups on the surface of magnetite.

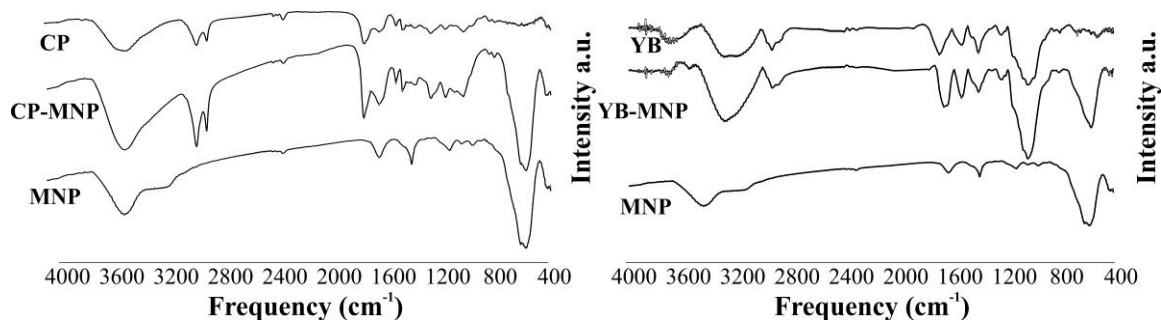


Figure 3. FT-IR spectra of CP (Cork powder), CP-MNP (ferromagnetic nanocomposites of cork powder), YB (yeast biomass); MNP-YB (yeast magnetic bionanocomposite) and MNP (magnetic nanoparticles).

3.2. Evaluation of methylene blue sorption

The SC_{exp} values for all adsorbents studied (Table 1) were assessed by their saturation, which was reached as the concentration of the supernatant, in the experiment bath, was the same as the initial work solution. These results of SC_{exp} were significantly different (one-way ANOVA and Tukey test). In this way, the order of sorption capacity among the adsorbents regarding SC_{exp} results and the efficient removal of methylene blue from solution is proposed. Thus, the methylene blue removing by the evaluated materials was $CP > CP-MNP > YB-MNP > YB \gg MNP$.

Table 1. Values of experimental Sorption Capacity (SC_{exp}), isotherms parameters and χ^2 error evaluation for sorption of methylene blue by CP-MNP (ferromagnetic nanocomposites of cork powder), CP (cork powder), YB (yeast biomass); MNP-YB (yeast magnetic bionanocomposite) and MNP (magnetic nanoparticles). CV = Coefficient of Variation, SD = Standard deviation, SE = Standard Error provided by fitting the model to the experimental data ($n = 3$).

	CP-MNP	CP	YB-MNP	YB	MNP
SC_{exp} (mg/g)	$33.6 \pm 0.9^{(SD)}$	$36.4 \pm 0.4^{(SD)}$	$30.4 \pm 0.9^{(SD)}$	$27.7 \pm 0.3^{(SD)}$	$2.9 \pm 0.4^{(SD)}$
Langmuir Model					
Q_{max} (mg/g)	$30 \pm 1^{(SE)}$	$25 \pm 1^{(SE)}$	$42 \pm 4^{(SE)}$	$46 \pm 3^{(SE)}$	$8710 \pm 7.37 \times 10^6^{(SE)}$
b (L/g)	$0.409 \pm 0.113^{(SE)}$	$0.177 \pm 0.053^{(SE)}$	$0.048 \pm 0.014^{(SE)}$	$0.031 \pm 0.004^{(SE)}$	$6 \times 10^{-6} \pm 0.005^{(SE)}$
r^2	0.9623	0.9633	0.9790	0.9927	0.9844
χ^2	5.03	2.49	2.36	5.38	0.01
Freundlich					
K	$6617 \pm 6823^{(SE)}$	$562 \pm 388^{(SE)}$	$22 \pm 22^{(SE)}$	$8 \pm 3^{(SE)}$	$0.037 \pm 0.001^{(SE)}$
n (L/mg)	$3.7 \pm 0.3^{(SE)}$	$3.7 \pm 0.2^{(SE)}$	$2.1 \pm 0.3^{(SE)}$	$1.8 \pm 0.1^{(SE)}$	$0.6102 \pm 0.0009^{(SE)}$
r^2	0.9876	0.9927	0.9526	0.9884	0.9991
χ^2	1.66	3.48	5.34	1.07	9.96×10^{-4}
SIPS					
Q_{max} (mg/g)	$132 \pm 347^{(SE)}$	$20 \pm 2^{(SE)}$	$31 \pm 2^{(SE)}$	$50 \pm 5^{(SE)}$	$2 \pm 1^{(SE)}$
K	$0.0006 \pm 0.0069^{(SE)}$	$0.0001 \pm 7 \times 10^{-8}^{(SE)}$	$0.08 \pm 0.01^{(SE)}$	$0.02 \pm 0.01^{(SE)}$	$24 \pm 5^{(SE)}$
n (L/mg)	$0.3 \pm 0.2^{(SE)}$	$-52 \pm 5 \times 10^{14}^{(SE)}$	$1.6 \pm 0.3^{(SE)}$	$0.9 \pm 0.2^{(SE)}$	$6 \pm 2 \times 10^{14}^{(SE)}$
r^2	0.9853	0.5083	0.9873	0.9919	-0.4531
χ^2	1.95	33.50	1.42	0.75	1.57

The performance of a sorbent can be evaluated by sorption isotherm data acquired experimentally. To choose which theoretical models would be tested, we classified the experimental isotherm according to Giles, which is suggested in the guidelines presented by [26]. From the experimental isotherms with a convex profile and a tendency to form a plateau due to the biosorbent saturation (Figure 4) and the use of proposed mathematic criteria we classified them as L1 or H1 (with no plateau) and L2 or H2 (with a plateau) [26, 27]. Based on this fact, we choose three non-linear isotherm models to determine the sorption isotherm parameters, such as Langmuir, Freundlich, and SIPS. While a sorption phenomenon purely chemical (described by Langmuir) or purely physical (defined by Freundlich) is rare, SIPS deals with the combination of these two adsorption models, and provides the same parameters as Langmuir and Freundlich

[27]. One of the information provided by a fitted model is the r^2 , which indicates the predominance of a given model in order to describe the characteristics of the sorption phenomena.

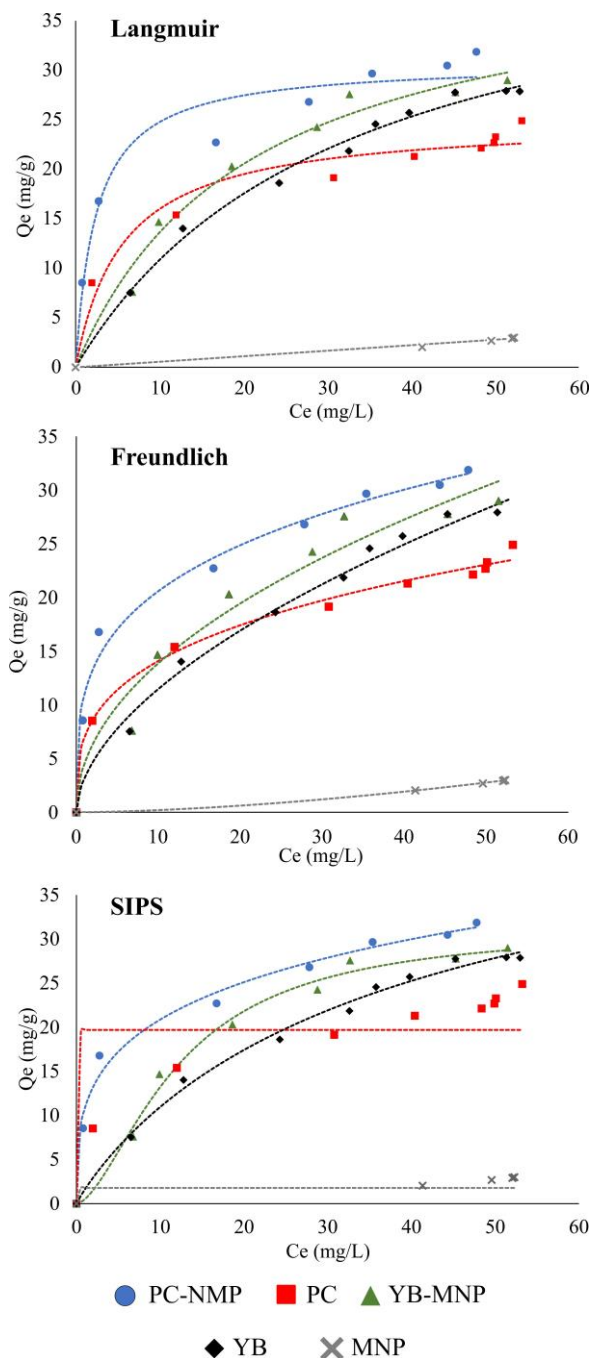


Figure 4. Adsorption curves and the Langmuir, Freundlich, and SIPS isotherms fitting for methylene blue sorption from water by CP (cork powder), CP-MNP (ferromagnetic nanocomposites of cork powder), YB (yeast biomass); MNP-YB (yeast magnetic bionanocomposite), and MNP (magnetic nanoparticles). $n = 3$.

Error functions also have been used to evaluate the error distribution between experimental data and theoretical predicted isotherm in an attempt to determine which of the various models available for evaluation adequately correlates the experimental data [4, 19, 28]. We chose the Chi-square test (χ^2) to evaluate the best fit of the non-linear theoretical models to the experimental data [29, 30]. Small values of χ^2 denotes higher similarities between the experimental isotherms and predict model [19].

Above and beyond, the fitted models offered parameters that allow to infer observations about the performance of a specific sorbent, such as maximum capacity, energy, and affinity of sorption. So, it is important to evaluate the standard

errors (SE) for each parameter offered by fitted models to estimate and the accuracy of the evaluated isotherm models in predicting them [28].

In this manner, we have established steps to consider the issues discussed above for the analysis of the adherence of experimental data to the theoretical models, in order to establish a model assignment which describe the phenomenon of observed sorption:

- (1) Perform the experiment in order to reach the saturation of the material and determine SC_{exp} ;
- (2) Trace the isotherm with the experimental data, evaluate of which class it belongs to and determine the indicated theoretical models to suite the best fit;
- (3) Apply the chosen theoretical models and obtain the values of r^2 , χ^2 (with their respective degrees of freedom) and the parameters provided by the models with their respective Standard Error (S.E.);
- (4) Select models with χ^2 lower than the critical value and if this condition is not suitable, other models should be run by returning to the step 2;
- (5) Within the set of models that meet step 3, select which one shows r^2 closer to 1 and also the smaller χ^2 value (it is possible that these conditions are satisfied by different models);
- (6) Confronting the defined models in step 4, considering the S.E. provided by each model, in order to define a model that describe the phenomenon of sorption observed and that presents parameters with smaller S.E.

After completing steps 1 and 2, step 3 was conducted, in which the experimental data adjustment to the theoretical models reflected degrees of freedom (d.f.) that varied between 5 and 8, which have the critical values of χ^2 varying between 11.070 and 15.507 ($\alpha = 0.05$). In this way, all models could be acceptable for describing the experimental data, except for SIPS for CP, which was discarded. Following to step 3, considering solely r^2 values (Table 1), we denote that just the model of SIPS for CP and MNP has a weak relationship to describe the experimental data. Nevertheless, as r^2 values closer to 1 correspond to stronger/plain fitting the models that could be assigned to describe the studied sorption phenomena for each material would be CP-MNP (Langmuir), CP (Freundlich), YB-MNP (SIPS), YB (SIPS) and MNP (Freundlich). On the other hand, considering the minor values of χ^2 the models that could predict the sorption of methylene blue from each sorbent material would be: CP-MNP (Freundlich), CP (Langmuir), YB-MNP (SIPS), YB (SIPS), and MNP (Freundlich). It is possible to verify that the models change if r^2 and χ^2 are individually considered to assign a theoretical model, that more adequately describes the observed sorption phenomena, thus, step 6 was applied.

Observing the SE values provided by fitting the experimental data to the isotherm models and confronting them with the attributions of theoretical models established by the isolated observation of r^2 and χ^2 , we suggest that the most adequate assignment for the description of the observed sorption phenomenon for each material would be CP-MNP (Langmuir), CP (Langmuir), YB-MNP (SIPS), YB (SIPS) and MNP (Freundlich). This is due to the K values of the Freundlich model for CP-MNP and CP, which show high SE. Besides, it is reasonable that the precursor biomasses and their composite materials exhibit similar behavior. The attributed models can explain the order of methylene blue removal efficiency by these materials established by SC_{exp} since the Langmuir model describes sorption involving energy of chemical bonds, Freundlich depicts electrostatic attraction between sorbent and sorbate, and SIPS indicates a contribution of both types of interaction [30].

Judging whether or not an adsorbent is efficient for the removal of a certain species is not a trivial task. It depends on the conditions in which the phenomena occur and the goals of the process [23], that is, if the interest is to uptake the largest quantity of an adsorbate present in solution, we must pay attention to the values of SC_{exp} and Q_{max} (Theoretical Maximum Sorption Capacity). However, it is possible that the same adsorbent does not behave as the most efficient in the removal of the species of interest along the whole concentration range studied. This may lead to a situation where a given adsorbent acts better at low concentrations than another, rather than having a lower SC_{exp} or Q_{max} [23].

In addition, it is important to consider the profile of the sorption isotherm curve and its initial slope. The lower the angle between the initial range of the curve and the y-axis, the higher the sorption affinity among the adsorbent and the species to be removed from the solution. Affinity between the sorbent and sorbate is provided by the coefficient b of the Langmuir equation, and the lower the b , the higher the sorption affinity [23]. Thus, by performing a visual evaluation of the initial slope we have the following order of sorption affinity: CP-MNP > CP > YB-MNP > YB >>> MNP. An opposite response was observed in relation to the order defined by SC_{exp} , in which CP > CP-MNP. This suggests that, by comparing the composite with its precursor biomass, it would be more suitable to remove methylene blue from water solutions if the adsorbate is present in low concentration. In our experiments, SC_{exp} and Q_{max} from attributed isotherm

models were the same for both composites. The Fe^{3+} in the nanoparticles contributes to the reduction of the surface tension between the sorbent and the water, favoring the interaction with the species to be removed [31].

The low SC_{exp} of MNP is due to the fact that they have surface covered by positive charges, which repel the molecules of methylene blue, which is a cationic dye [8, 32]. On the other hand, biological materials present chemical structures rich in sorption sites with negative charges, which favors the uptake of positively charged species present in solution, and explains the high removal of methylene blue by CP and YB [23]. It is interesting to notice that the performance of the composites was not affected by the presence of ferromagnetic nanoparticles (MNP), allowing them to present the sorption characteristics related to the biomasses associated to the magnetic characteristics that favored an efficient removal of CP-MNP and YB-MNP from the solution by the simple application of a magnetic field, which contributes to its application in real situations [33]. This fact denotes that composites are hybrid materials that present distinct characteristics of their precursors, each preserving its positive potentials and the new attributes.

It is important to mention that the methylene blue solution pH was 9.03 ± 0.01 , in which its molecule is deprotonated ($\text{pK}_a = 3.8$). At the end of the sorption process, the supernatants pHs were lower (CP-MNP = 6.66 ± 0.01 , CP = 6.34 ± 0.01 , YB-MNP = 6.23 ± 0.01 , YB = 6.17 ± 0.01 , and MNP = 5.99 ± 0.01). This indicates that the removal of the dye displaces H^+ ions from the surface of the adsorbent by substitution for methylene blue [34].

3.3. Textile effluent (TE) sorption

The amount of dyes removed from the effluent was 6.7 ± 0.4 , 14.2 ± 0.5 , 10.9 ± 0.5 , and 13 ± 2 mg/g for CP-MNP, CP, YB-MNP, and YB, respectively. These values were lower than expected, considering the methylene blue SC_{exp} denoting that the treatment of an actual effluent present different conditions to be considered. First, in a real effluent there is no controlled conditions and part of the dyes are not in the original form, since the dyeing process promotes their hydrolysis [35]. Furthermore, the textile effluent is composed of a trichomy of dyes which can compete with one another for the sorption sites available, a fact that can lead to the prevalence of sorption of one dye over another [36]. Besides, the effluent matrix is rich of cations and anions, which increases the ionic strength of the medium leading to a double-layer effect (Helmholtz layer) that difficult the approximation of the dye residues in the effluent to the sorbents surfaces [37].

Another possible explanation for the lower removal of dyes from the effluent may be associated with the effluent pH, since this is an important parameter in the sorption processes acting on protonation or deprotonation of sorption sites and adsorbate species [38]. The initial effluent pH was 6.94 and at the end of the sorption this value changed to = 7.52, 7.41, 5.85 and 6.86 for CP, CP-MNP, YB and YB-MNP, respectively. As the structural formula of dyes were not disclosed, due to patent protection, it is not possible to predict if at these pHs the dyes are protonated or not. Therefore, it is known that at lower pH the availability of H^+ ions can compete with the adsorbates to the sorption sites, becoming unavailable to the sorption process [23]. It is interesting to note that for CP and CP-MNP the final pHs were higher than the initial, suggesting a consumption of H^+ ions during the sorption process, which may be related to the capture of H^+ by some process coming from the sorption mechanisms.

In an attempt to improve the removal of the remaining dyes from the effluent, a mass variation study was carried out. Figure 5 presents the amounts of removed dye from the effluent employing different masses of each evaluated sorbent material.

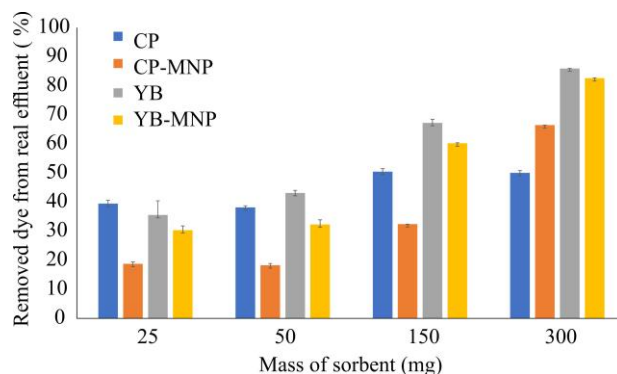


Figure 5. A) Removal dye from real effluent by CP-MNP (ferromagnetic nanocomposites of cork powder), CP (cork powder), YB (yeast biomass); MNP-YB (yeast magnetic bionanocomposite) and MNP (magnetic nanoparticles), $n = 3$.

In general, it is possible to observe an increment in the amount of the dyes removed with the increase of the sorbent mass employed and a better response of YB and YB-MNP, differently from what was observed for methylene blue, which showed higher sorption by CP and CP-MNP. The ANOVA following Tukey test ($\alpha = 0.05$) showed similarities among: a) CP and YB (25 mg) and CP and YB (50 mg); b) YB (25 mg), CP (50 mg), YB-MNP (50 mg) and CP-MNP (150 mg); c) YB-MNP (50 mg) and CP-MNP (150 mg); d) CP (150 mg) and CP (300 mg); and YB (150 mg) and CP-MNP (300 mg). It is difficult to describe a consistent behavior. However, it is relevant to report that the actual effluent treatment in the sorbent studies were feasible since the removal of the dyes reached up to $50.0 \pm 0.8\%$ (CP), $66.48 \pm 0.01\%$ (CP-MNP), $85.93 \pm 0.07\%$ (YB) and $82.6 \pm 0.1\%$ (YB-MNP).

4. Conclusions

The assignment of a theoretical model to describe a sorption phenomenon employing criteria established by a logic based on the main parameters that delineate an appropriate fit can facilitate the decision of the analyst, respectively r^2 provided for the adjusted model, the error of fit of the model (regardless the error function chosen for the verification), and finally the values of Standard Error (SE) provided by the model adjusted for each parameter that compose it. It is also important that the procedure promotes the saturation of the biosorbent, which actually allows to establish the SC_{exp} of the studied material, which can be compared with the values of Q_{max} , avoiding that a sorbent material is taken as having high sorption capacity, but only in theoretical data that may be associated to an improperly fitted model, not meeting reliability criteria of its adjustments and that may cause distortions of interpretation. Studies involving controlled systems, that is, with standard solutions prepared in the laboratory, do not reflect the behavior of a sorbent against the actual conditions of treatment of textile effluents whose complexity may interfere in the sorption process, necessitating adjustments for an effective positive response. In addition, it can be concluded that nanoferrromagnetic composites offer the combination of characteristics of their precursors, which, together, allow the removal of species of interest from the aqueous medium and separation of the sorbent and the effluent quickly and quantitatively.

Acknowledgements: The authors acknowledge the financial support from Fapesp, Processo 2016/0627-4 and are grateful to UNESPetro (Rio Claro - SP) and Centro Experimental multiusuário da Universidade Federal do ABC.

5. References

1. Robinson, T., McMullan, G., Marchant, R., Nigam, P.: Remediation of dyes in textile effluent: a critical review on current. *Bioresource Technol.* 77, 247-255 (2001)
2. Rahman, F.: The treatment of industrial effluents for the discharge of textile dyes using by techniques and adsorbents, *J. Textile Sci. Eng.* 6, 1-9 (2016)
3. Kehinde, F.O, Aziz, H.A.: Textile Waste Water and the advanced Oxidative Treatment Process, an Overview. 3, 15310-15317 (2014)
4. Amrhar, H.N., Elyoubi, M.S.: Application of nonlinear regression analysis to select the optimum absorption isotherm for Methylene Blue adsorption onto Natural Illitic Clay Otheman. *B. Soc. Roy. Sci. Liège* 84, 116-130 (2015)
5. Safaricová, M., Ptácková, K., Kibriková, I., Safarik, I.: Biosorption of water-soluble dyes on magnetically modified *Saccharomyces cerevisiae* subsp. *uvarum* cells. *Chemosphere* 59, 831-835 (2005)
6. Yu, B.Y., Kawk, S.Y.: Assembly of magnetite nanocrystals into spherical mesoporous aggregates with a 3-D wormhole-like pore structure. *J. Mater. Chem.* 20, 8320-8328 (2010)
7. Jiang, R., Tian, J., Zheng, H., Qi, J., Sun, S., Li, X.: A novel magnetic adsorbent based on waste litchi peels for removing Pb(II) from aqueous solution. *J. Environ. Manage.* 155, 24-30 (2015)
8. Tan, K.A., Morad, N., Teng, T.T., Norli, I., Paneerselvam, P.: Removal of cationic dye by magnetic nanoparticle (Fe_3O_4) impregnated onto activated maize cob powder and kinetic study of dye waste adsorption. *APCBEE Procedia* 1, 83-89 (2012)
9. Saber, O., Mohamed, N.H., Arafat, S.A.: Conversion of iron oxide nanosheets to advanced magnetic nanocomposites for oil spill removal. *RSC Adv.* 5, 72863-72871 (2015)
10. Labuto, G., Carrilho, E.N.V.M.: Bioremediation in Brazil: scope and challenges to boost up the Bioeconomy. In: Prasad, M.N.V. (ed.). *Bioremediation and Bioeconomy*, pp. 569-586. Elsevier, Oxford (2016)
11. Behrens, S.: Preparation of functional magnetic nanocomposites and hybrid materials: recent progress and future directions. *Nanoscale* 3, 877-892 (2011)

12. Pirbazari A.E., Saberikhah E., Kozani, S.S.H.: Fe₃O₄-wheat straw: preparation, characterization and its application for methylene blue adsorption. *Water. Res. Ind.* 8, 23-27 (2014)
13. Madrakian, T., Afkhami, A., Ahmadi, M.: Adsorption and kinetic studies of seven different organic dyes onto magnetite nanoparticles loaded tea waste and removal of them from wastewater samples. *Spectrochim. Acta A* 99, 102-109 (2012)
14. Wong, K.T., Eu, N.C., Ibrahim, S., Kim, H., Yoon, Y., Jang, M.: Recyclable magnetite-loaded palm shell-waste based activated carbon for the effective removal of methylene blue from aqueous solution. *J. Clean Prod.* 115, 337-342 (2016)
15. Makarchuk, O.V., Dontsova, T.A, Astrelin, I.M.: Magnetic nanocomposites as efficient sorption materials for removing dyes from aqueous solutions. *Nanosc. Res. Lett.* 11, 161-167 (2016)
16. Tim, C.: Remarks on adsorption manuscripts received and declined: An editorial. *Separation and Purification Tehchnol.* 54, 277-278 (2007)
17. Molina M.M., Seabra A.B., Oliveira M.G., Itri, R., Haddad P.S.: Nitric oxide donor superparamagnetic iron oxide nanoparticles. *Mater. Sci. Eng. C. Mater. Biol. Appl.* 33, 746-751 (2013)
18. Panneerselvam, P., Morad, N., Tan, K.: Magnetic nanoparticle (Fe₃O₄) impregnated onto tea waste for the removal of nickel(II) from aqueous solution. *J. Hazard. Mat.* 186, 160-168 (2011).
19. Subramanyam, B., Das, A.: Linearised and non-linearised isotherm models optimization analysis by error functions and statistical means. *J. Environ. Health. Sci. Eng.* 12, 92-98 (2014)
20. Klug, H.P., Alexander, L.E.: X-Ray diffraction procedures: for polycrystalline and amorphous materials. John Wiley & Sons, New York (1974)
21. Fudimura, K.A., Seabra, A.B., Santos, M.D.C., Haddad, P.S.: Superparamagnetic iron oxide nanoparticles dispersed in Pluronic F127 hydrogel: potential uses in topical applications. *J. Nanosci. Nanotechno.* 17, 133 (2017)
22. Kumar, R., Inbaraj, B.S., Chen, B.H.: The synthesis and characterization of poly(γ -glutamic acid)-coated magnetite nanoparticles and their effects on antibacterial activity and cytotoxicity. *Mater. Res. Bull.* 45, 1603-1608 (2010)
23. Volesky, B.: Sorption and biosorption, Québec: BV Sorbex, 2003
24. Silva, S.P., Sabino, M.A., Fernandes, E.M., Correlo, V.M., Boesel, L.F., Reis, R.L.: Cork: properties, capabilities and applications. *Int. Mat. Rev.* 50, 345-365 (2005).
25. Wang, J., Chen, C.: Biosorption of heavy metals by *Saccharomyces cerevisiae*: a review. *Biotechnol. Adv.* 24, 427-451 (2006)
26. Hinz, C.: Description of sorption data with isotherm equations. *Geoderma* 99(3-4), 225–243 (2001)
27. Limousin, G., Gaudet, J.P., Charlet, L., Szenknect, S., Barthe's V., Krimissa, M.: Sorption isotherms: a review on physical bases, modeling and measurement. *App. Geochem.* 22, 249-275 (2007)
28. Chen, X.: Modeling of Experimental Adsorption Isotherm Data, *Information* 6, 14-22 (2015)
29. Foo, K.Y., Hameed, B.H.: Insights into the modeling of adsorption isotherm systems. *Chem. Eng. J.* 156, 2-10 (2010)
30. Chen, C.: Evaluation of equilibrium sorption isotherm equation. *Open. Chem. Eng. J.* 7, 24-44 (2013)
31. Dabrowski, A.: Adsorption--from theory to practice. *Adv Colloid Interface Sci.* 93, 135-224 (2001)
32. Fard, A.K., Rhadfi, T., Mckay, G., Al-Marri, M., Abdala, A., Hilal, N., Hussiena, M.A.: Enhancing oil removal from water using ferric oxide nanoparticles doped carbon nanotubes adsorbents. *Chem. Eng. J.* 293, 90-101 (2016)
33. Illés, E., Tombác, E.: The effect of humic acid adsorption on pH-dependent surface charging and aggregation of magnetite nanoparticles. *J. Colloid Interf. Sci.* 295, 115-123 (2006)
34. Yu, J.X., Wang L.Y., Chi, R.A., Zhang, Y.F., Xu, Z., Guo, J.: A simple method to prepare magnetic modified beer teas and it is application for cationic dye adsorption. *Env. Sci. Pol. Res.* 20, 543-551 (2013)
35. Schiewer, S., Fourest, E., Chong, K.H., Volesky, B.: Ion exchange in biosorption by dried seaweed: experiments and model predictions. In: Jerez, C.A., Vargas, T., Toledo, H., Wiertz, J.V. (eds.) *Biohydrometallurgical Processing*, pp.219-228. Univ. Chile, Santiago (1995)
36. Karcher, S., Kornmüller, A., Jekel, M.: Screening of commercial sorbents for the removal of reactive dyes. *Dyes Pigments* 51, 111–125 (2001)
37. Chen, C-Y., Chang, J-C., Chen, A-H.: Competitive biosorption of azo dyes from aqueous solution on the templated crosslinked-chitosan nanoparticles. *J. Hazard. Mat.* 185, 430-441 (2011)
38. Schiewer, S., Volesky, B.: Strength and electrostatic effects in biosorption of divalent metal ions and protons. *Environ. Sci. Technol.* 31, 2478-2485 (1997)

39. Bian, S.W., Mudunkotuwa, I.A., Rupasinghe, T., Grassian, V.H.: Aggregation and dissolution of 4 nm ZnO nanoparticles in aqueous environments: influence of pH, ionic strength, size, and adsorption of humic acid. *Langmuir* 27(10), 6059–6068 (2011)